

The 12 September 1999 Upper East Rift Zone dike intrusion at Kilauea Volcano, Hawaii

P. Cervelli,^{1,2} P. Segall,¹ F. Amelung,³ H. Garbeil,³ C. Meertens,⁴ S. Owen,⁵
A. Miklius,⁶ and M. Lisowski⁷

Received 27 April 2001; revised 10 September 2001; accepted 19 September 2001; published 31 July 2002.

[1] Deformation associated with an earthquake swarm on 12 September 1999 in the Upper East Rift Zone of Kilauea Volcano was recorded by continuous GPS receivers and by borehole tiltmeters. Analyses of campaign GPS, leveling data, and interferometric synthetic aperture radar (InSAR) data from the ERS-2 satellite also reveal significant deformation from the swarm. We interpret the swarm as resulting from a dike intrusion and model the deformation field using a constant pressure dike source. Nonlinear inversion was used to find the model that best fits the data. The optimal dike is located beneath and slightly to the west of Mauna Ulu, dips steeply toward the south, and strikes nearly east-west. It is approximately 3 by 2 km across and was driven by a pressure of ~ 15 MPa. The total volume of the dike was 3.3×10^6 m³. Tilt data indicate a west to east propagation direction. Lack of premonitory inflation of Kilauea's summit suggests a passive intrusion; that is, the immediate cause of the intrusion was probably tensile failure in the shallow crust of the Upper East Rift Zone brought about by persistent deep rifting and by continued seaward sliding of Kilauea's south flank.

INDEX TERMS: 7280 Seismology: Volcano seismology (8419); 8035 Structural Geology: Pluton emplacement; 8434 Volcanology: Magma migration; 8494 Volcanology: Instruments and techniques;

KEYWORDS: Kilauea, deformation, dike, intrusion, GPS, InSAR

1. Introduction

[2] On the morning of 12 September 1999 at 0131 LT (Hawaiian Standard Time, UT - 10) a swarm of small earthquakes and associated volcanic tremor began at Kilauea Volcano. The swarm was concentrated along the east rift zone near Mauna Ulu, but earthquakes eventually spread throughout a broader area including the summit and south flank (Figure 1). The largest earthquake of the swarm was about magnitude 3.0; however, ~ 4 hours after the swarm began a magnitude 3.7 earthquake occurred beneath Kilauea's south flank near the active vent, Pu'u 'O'o.

[3] Deflation at Kilauea's summit and at Pu'u 'O'o accompanied the swarm. The deflation, detected by electronic tiltmeters, began concurrently with the earthquakes

and tremor (Figure 2). Sometime between the beginning of the swarm and when observers arrived at the scene ~ 10 hours later (1100 LT) the floor of Pu'u 'O'o had collapsed, presumably in response to the rapid deflation. At this time, the flow of lava through the tube to the coast was observed to be weak and sluggish. By 1330 LT, the eruption had paused and did not resume again until nearly 11 days later on 23 September 1999 at approximately 1100 LT.

[4] This region of Kilauea's upper east rift zone has experienced many earthquake swarms, including a sequence in 1993 that caused extensive ground cracking and nearly resulted in the evacuation of Hawaii Volcanoes National Park. U.S. Geological Survey (USGS) topographic maps of the area show additional ground cracks that formed prior to the 1993 intrusion. No eruptions have occurred in this area since the Mauna Ulu eruptions of the early 1970s.

[5] Earthquake swarms in or near Kilauea's rift zones, particularly when accompanied by harmonic tremor and summit deflation, are typically interpreted as dike intrusions. This interpretation seems plausible given that (1) harmonic tremor almost certainly results from fluid flow; (2) deflation of the summit is indicative of exiting magma; and (3) fissure eruptions are almost invariably accompanied by both tremor and summit deflation. In the analysis that follows, we present and model geodetic data that strongly suggest that the September 1999 earthquake swarm resulted from the intrusion of a 3 by 2 km, subvertical, east-west striking dike with a total volume of $\sim 3.3 \times 10^6$ m³. The dike was located just to the west of Mauna Ulu and came to within ~ 0.5 km of the surface. The geodetic data also imply

¹Department of Geophysics, Stanford University, Stanford, California, USA.

²Now at U.S. Geological Survey, Hawaiian Volcano Observatory, Hawaii National Park, Hawaii, USA.

³Department of Geology and Geophysics, University of Hawaii at Manoa, Honolulu, Hawaii, USA.

⁴University NAVSTAR Consortium, Boulder, Colorado, USA.

⁵Department of Earth Sciences, University of Southern California, Los Angeles, California, USA.

⁶U.S. Geological Survey, Hawaiian Volcano Observatory, Hawaii National Park, Hawaii, USA.

⁷U.S. Geological Survey, Cascades Volcano Observatory, Vancouver, Washington, USA.

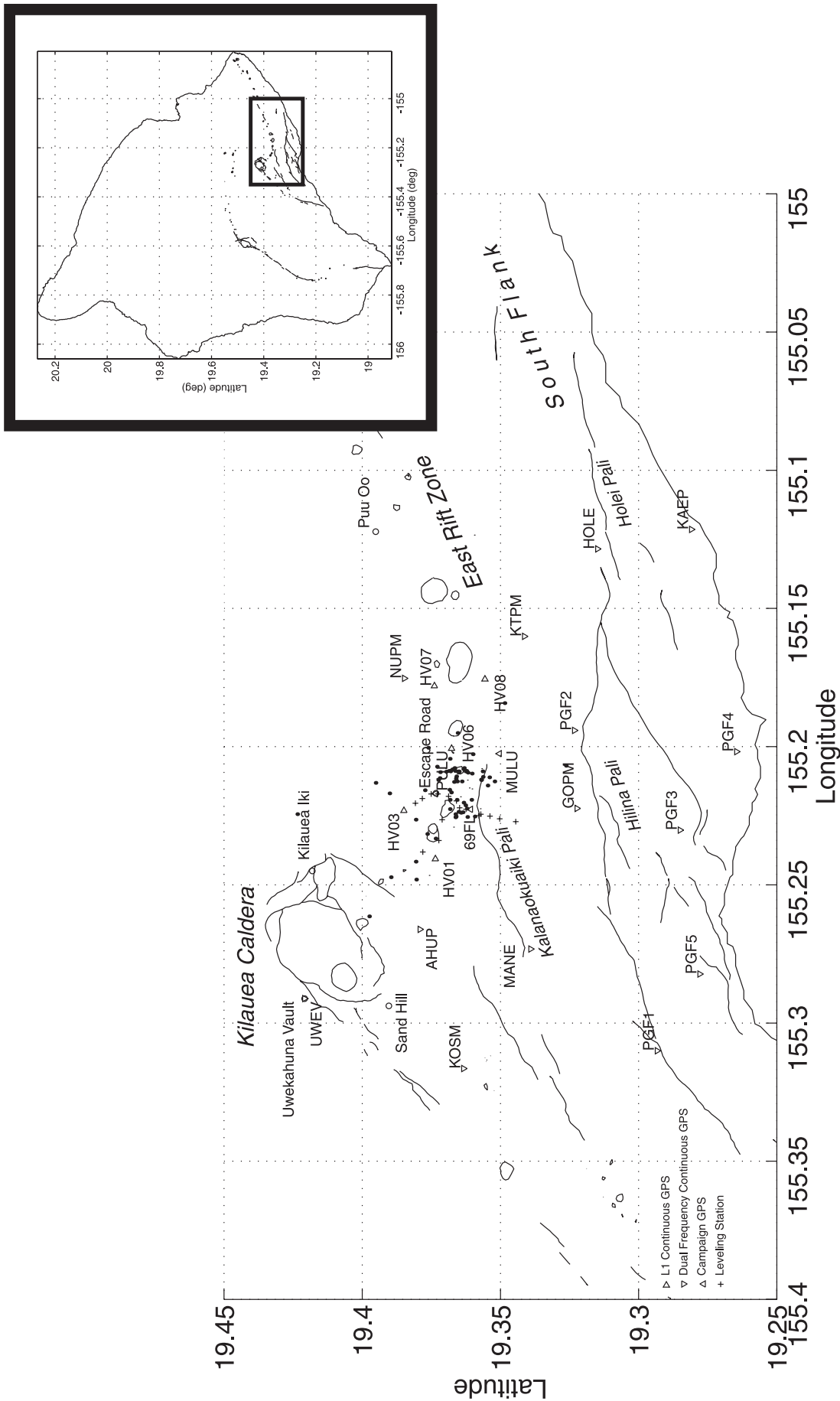


Figure 1. An overview of Kilauea Volcano, its caldera, and upper east rift zone. South pointing triangles mark the locations of the dual-frequency GPS receivers; east pointing triangles denote the single-frequency GPS receivers; north pointing triangles denote the campaign GPS stations; circles denote the tiltmeters; and crosses denote leveling bench marks. The small points are the hypocenters from the September 1999 earthquake swarm. The inset shows the location of the depicted region on the Big Island of Hawaii.

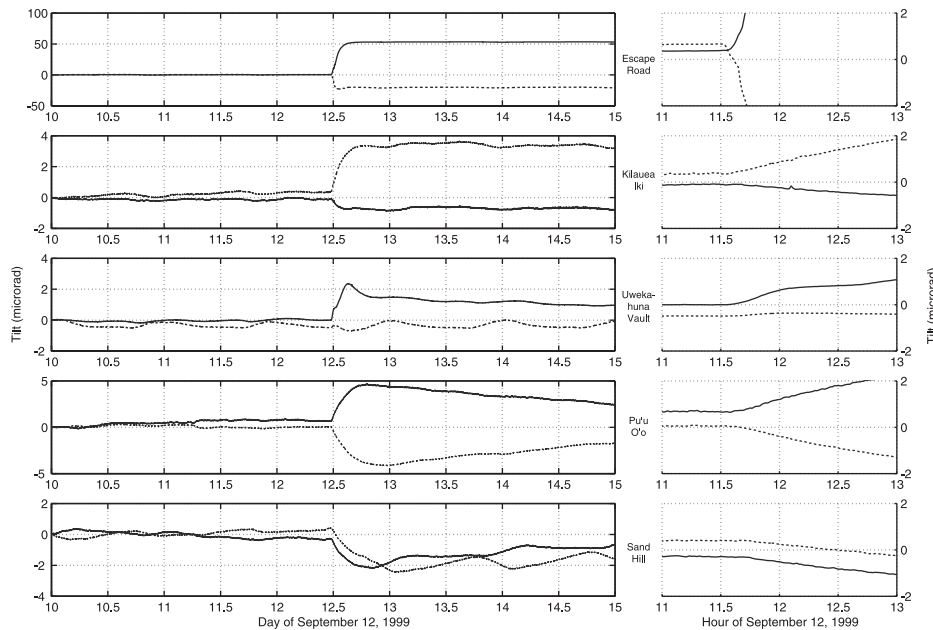


Figure 2. Time series from five borehole tiltmeters on Kilauea Volcano. The solid line shows the east component, the dashed line shows the north component. The sign of the tiltmeter is opposite from the gradient of the vertical deformation field; that is, positive tilt is down to the north and east. (left) A 5-day period surrounding the 12 September 1999 earthquake swarm. (right) Hours immediately before and after the beginning of the swarm.

that the dike propagated from west to east and that the magma source was the magma chamber beneath Kilauea Caldera.

2. Data

[6] The earthquake swarm occurred in a region of Kilauea Volcano monitored by continuously recording Global Positioning System (GPS) receivers and by borehole tiltmeters. Additional geodetic data consists of campaign-mode GPS, precise leveling, and measurements from the ERS interferometric synthetic aperture radar (InSAR) satellite.

2.1. GPS

[7] Stanford University, the Hawaiian Volcano Observatory (HVO), and the University of Hawaii operate a network of continuously operating dual-frequency GPS receivers on Kilauea Volcano (Figure 1, south pointing triangles). In June 1999 the University NAVSTAR Consortium (UNAVCO) deployed an experimental network of 12 inexpensive single frequency (L1) receivers (Figure 3, east pointing triangles). Stanford and HVO also conduct yearly campaign-mode GPS surveys. Three of the stations from the campaign network were near enough to the earthquake swarm to record an unambiguous signal (Figure 1, north pointing triangles). The dual-frequency GPS data were processed with Gipsy/Oasis II at HVO, using a fiducial-free, precise point-positioning strategy, which produces solutions in the ITRF96 reference frame [Zumberge *et al.*, 1997]. A coordinate time series for a site (GOPM) near the September 1999 swarm is shown in Figure 4. We estimate displacements from these data using weighted least

squares and propagate the observation errors to calculate the displacement covariance. The covariance is then scaled by the mean square error of the estimation. The estimated horizontal displacements and 95% confidence ellipses are depicted in Figure 3 in red.

[8] The L1 GPS data were processed together with a subset of the dual-frequency sites using Bernese at UNAVCO. The daily solutions are in a very loosely constrained reference system, so direct analysis of the coordinate time series as above is not possible. To circumvent this problem, we will model the baseline changes from the intrusion rather than absolute coordinate changes. The magenta vectors in Figure 3 depict the cointrusive baseline changes, here plotted relative to HVO1. The error ellipses grow with distance from HVO1 because the ionospheric path delay of the GPS signals cannot be eliminated with just single-frequency data. Thus the errors associated with L1 GPS data are, in general, larger than with dual-frequency systems. However, for short baselines (a few kilometers) the two nearby stations see essentially the same ionosphere, and the path error tends to cancel out, leaving only the lensing (scale) effect on the baseline lengths. Note that because the magenta vectors depicted in Figure 3 are plotted relative to HVO1, the error ellipses at the HVO7 and HVO8 are quite large. However, the uncertainty of the baseline between these two stations is actually very small. Thus plotting baseline changes with respect to a single station can imply misleadingly large errors. This is unfortunate but completely irrelevant to the modeling, provided that the full data covariance is used to weight the inversion.

[9] To estimate cointrusive displacements from the campaign GPS observations, it is necessary to detrend the coordinate time series, since significant deformation not

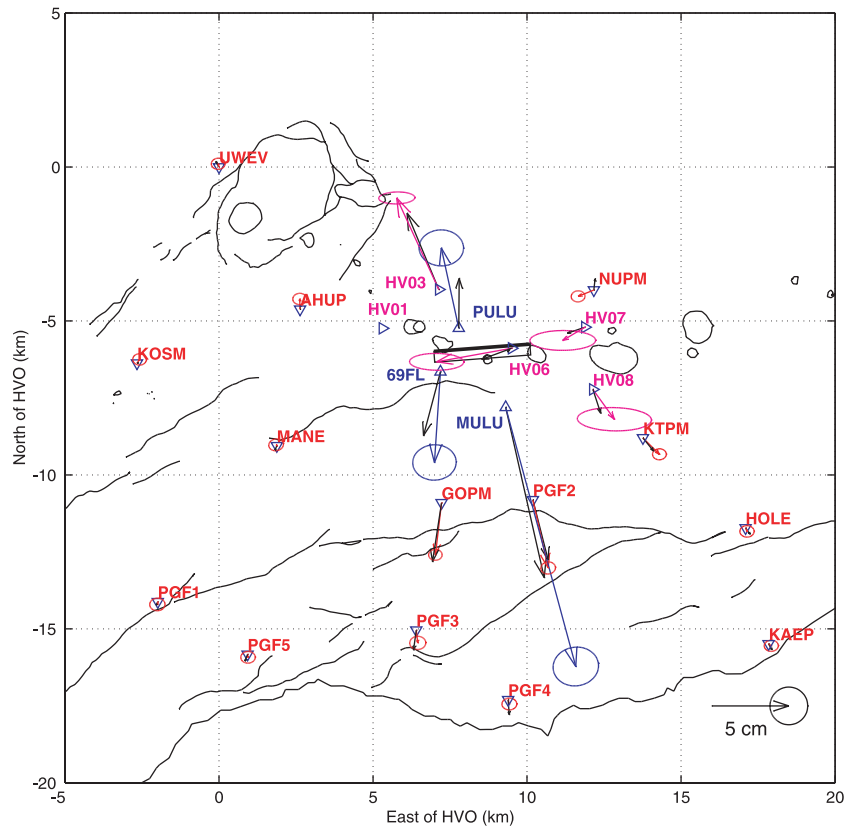


Figure 3. Observed and predicted data from the 12 September 1999 dike intrusion. Black vectors are the model prediction. Red vectors are the dual-frequency continuous sites; blue vectors are the campaign sites; magenta vectors are the L1 only continuous sites, plotted relative to HV01. Error ellipses are 95%.

directly related to the intrusion occurs between campaigns. So, as above we use weighted least squares to estimate the cointrusive displacements and (scaled) covariance, but we also estimate the nuisance parameters representing the secular trend. Figure 5 depicts time series from the three campaign stations used in this analysis. Though campaign data are available for these stations stretching back to the early 1990s, we chose to use data dating back only to mid-1997, since the east rift zone eruption of 30 January 1997 caused significant perturbations to the otherwise quasi-steady deformation rates [Owen *et al.*, 2000b]. The estimated displacements from the campaign data are shown in Figure 3 in blue.

2.2. Leveling

[10] Leveling surveys are performed yearly along a 16-station line that runs through the swarm area (Figure 6). Immediately after the 12 September swarm, a crew from HVO releveled the line, which had last been surveyed on 14 April 1999. The interval between the two surveys is long enough that the leveling data must be detrended like the campaign GPS data discussed above. We use annual leveling surveys from mid-1997 to 1999 plus an additional survey taken just after the intrusion to estimate cointrusive height changes and the (nuisance) height change trend. The estimated cointrusive height changes with respect to the northernmost station of the leveling line, HVO95, are shown in Figure 7. The errors in the estimated height changes were

calculated by stipulating a standard error of $\sigma = 1.20 \text{ mm} \sqrt{\text{km}}$ for the leveling measurements themselves and by then scaling the estimate covariance matrix by the mean square error of the estimation as above. Because leveling data are highly correlated with one another, it is quite important to use the full data covariance to appropriately weight the data when modeling. To calculate the correlations we use the method of *Arnadóttir et al.* [1992].

2.3. InSAR

[11] We formed an interferogram using ERS-2 InSAR images from 16 September 1998 and 23 February 2000 (perpendicular baseline 64 m). The InSAR data were down linked at the satellite ground station operated by the University of Hawaii. The topographic phase was removed using a U.S. Geological Survey digital elevation model. Figure 8a depicts the observed unwrapped range change in the direction of the satellite. Because most of Kilauea's southeast flank is covered with recent lava flows the interferometric coherence is generally very high.

[12] The cointrusive displacement signal in the interferogram is biased by 18 months of secular deformation. To minimize the effect of this bias, we use the dislocation model of *Owen et al.* [2000b] to predict and remove the accumulated range change during the 18-month interval. The predicted secular range change is depicted in Figure 8b and the difference between Figures 8a and 8b, i.e., the detrended range change, is shown in Figure 8c. Note that

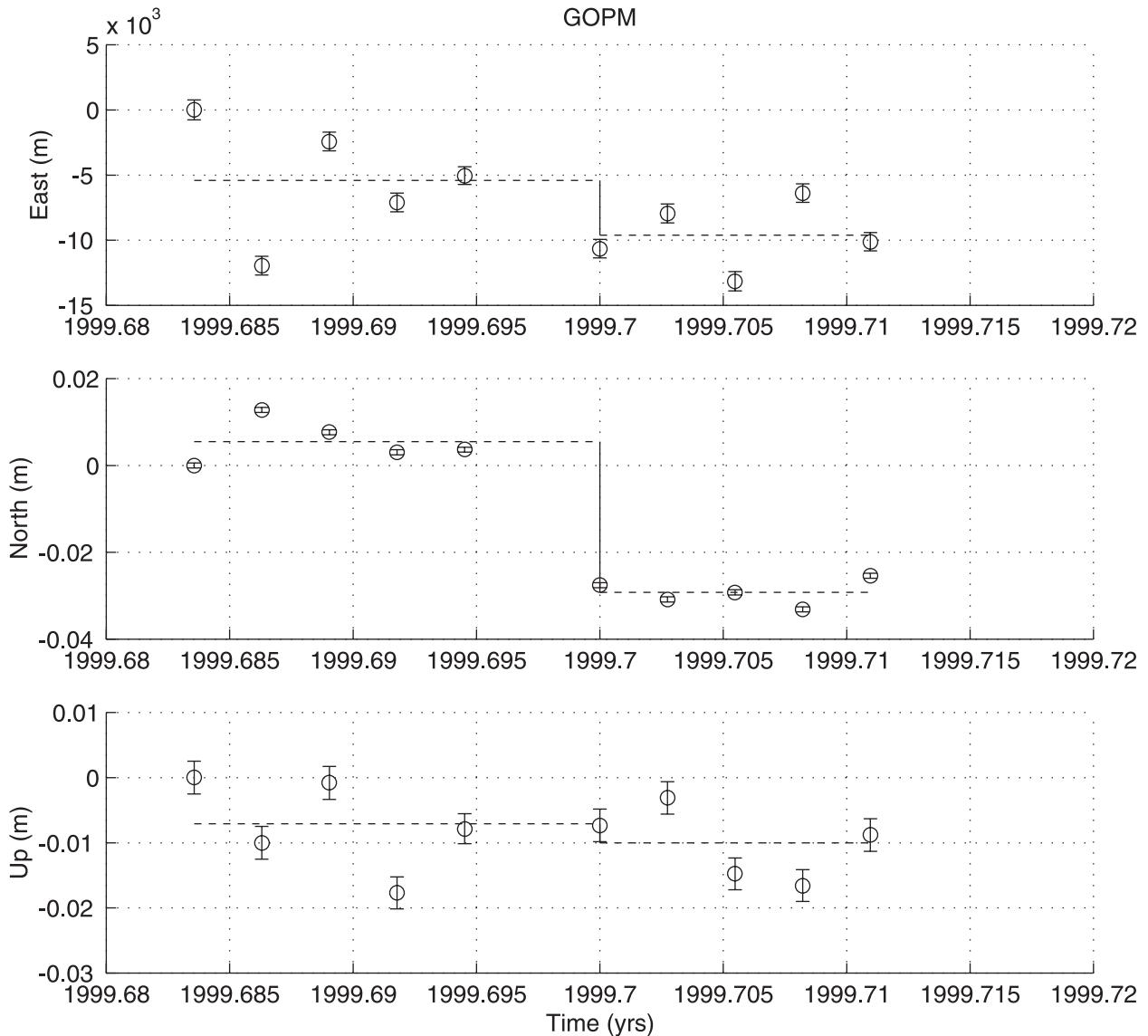


Figure 4. Time series for dual-frequency continuous site GOPM. Horizontal lines show that static position; vertical line is the estimated cointrusive displacement.

in the areas of the south flank distant from the earthquake swarm, the detrended range changes are close to zero, as we would expect if the dislocation model is doing a good job of predicting the secular trend in this region. It appears, however, that at the southernmost part of the south flank, the dislocation model is probably overpredicting the range change. Since this region is quite distant from the earthquake swarm, we can justifiably ignore it for the purposes of modeling a dike intrusion in the upper east rift zone. We therefore crop the range change data to a region close to the swarm and where the secular correction appears to be adequate. To make the InSAR data more computationally manageable, we down-sampled the image in Figure 8c using a quad-tree algorithm [Welstead, 1999]; the 268 points that were actually used in the modeling are shown as red dots.

2.4. Tilt

[13] Five borehole tiltmeters showed significant signals from the earthquake swarm (Figures 1 and 2). While these

instruments can be extremely precise, we chose not to include the tilt data in the formal inversion for dike geometry that follows. This decision stemmed from several factors: First, all of the tiltmeters contain a signal not just from the dike intrusion itself but also from the secondary effect of subsiding magma reservoirs. Second, the tiltmeter with the largest signal, Escape Road, is contaminated by sizable jumps associated with the larger earthquakes in the swarm (Figure 2). These jumps probably do not represent elastic deformation caused by the earthquakes (indeed, they are much too large to have originated from earthquakes of these magnitudes). Rather, the jumps probably reflect settling of the instrument within its casing (M. Johnston, personal communication, 2000). Finally, there is some uncertainty ($\pm 5^\circ$) in the orientation of the tiltmeter axes with respect to the geographic directions and also uncertainty in the calibration factor ($\pm 5\%$) between instrument “counts” and microradians. We do not discard the tilt data, however; we will

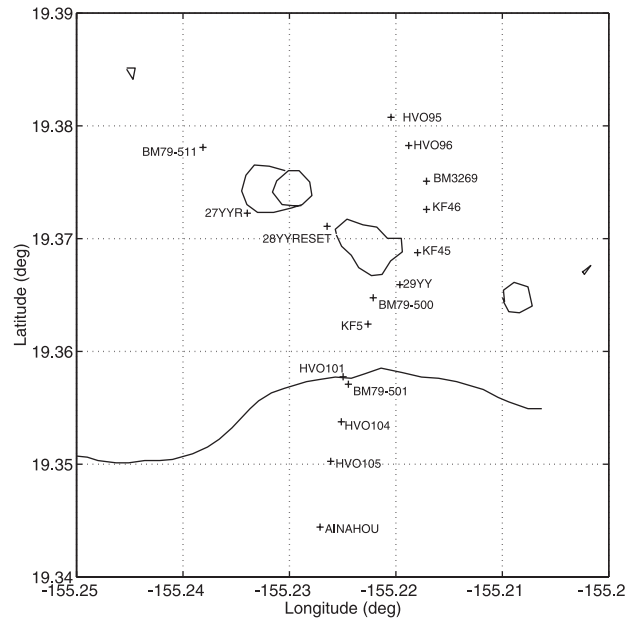
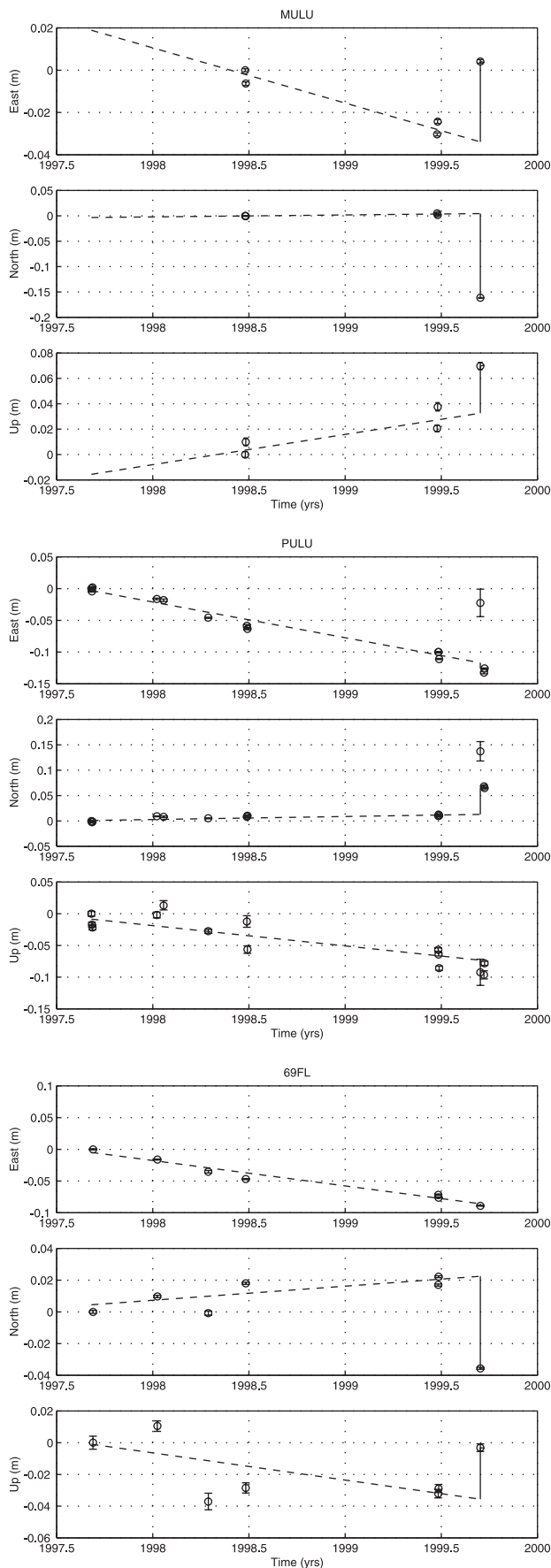


Figure 6. The Escape Road leveling line near the upper east rift zone, Kilauea Volcano. The crosses mark the leveling bench marks.

use them later to infer the direction and timing of dike propagation.

3. Model

[14] On the basis of the symmetry of the deformation field (Figure 3), the locations of the earthquake hypocenters, and the geological setting of the swarm area, we chose to model this event as a dike intrusion using uniform, opening-mode dislocations. As mentioned above, several tiltmeters show an unmistakable signal related to subsiding magma chambers. We chose not to model these magma chambers, however, for two reasons: the cointrusive displacements estimated from the GPS and leveling data, and the range changes from the InSAR data span a long enough interval to give the magma chambers plenty of time to refill, and even in the case of the continuous GPS data, which may be temporally dense enough to resolve the subsidence, the signal-to-noise ratio at sites near subsiding areas is very low.

[15] The initial modeling step is to find the single uniform opening dislocation that minimizes the difference between the observed and predicted deformation fields. (We assume a homogeneous elastic half-space and use the analytic expressions for the predicted deformation from

Figure 5. (opposite) Time series from the three campaign GPS sites used in this analysis. The sloped lines are the secular velocities of the sites, while the vertical lines are the estimated cointrusive displacements. The interval for estimating the secular trend extends back only to the second half of 1997 to avoid the effect of the episode 54 eruption of January 1997.

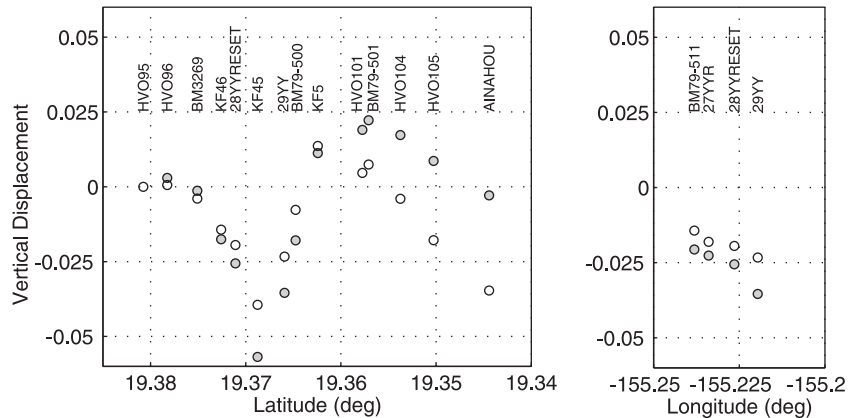


Figure 7. The observed (open) and predicted (solid) height changes along the Escape Road leveling line.

Okada [1985, 1992].) This inverse problem can be cast as an optimization, which can be solved with nonlinear optimization tools. In particular, we run two Monte Carlo algorithms, simulated annealing and random cost [Cervelli *et al.*, 2001]. Because of the disparate data sets involved in the inversion it is important to weight each different data set appropriately. We are fairly confident that the covariances of the GPS and leveling are correct. The covariance of InSAR data, however, is not known, so we assumed covariance of the form $\sigma^2 \mathbf{I}$. We used $\sigma = 0.02$ m since this was the scale of the scatter about the mean of the detrended interferogram. Combining the covariances of the different data sets into a single matrix, Σ_d , permits us to form the weight matrix: $\mathbf{W} = \Sigma_d^{-1}$, which is used to weight the residual sum of squares from a candidate model.

[16] Once we are confident that we have found the best fitting uniform opening dislocation, we switch to a more complex source model that has constant driving pressure rather than constant opening. To approximate the deformation field from a constant pressure dike, we use a boundary element method that involves discretizing the single dislocation into patches and then solving for a slip distribution that results in a constant normal stress on every patch. To make the problem computationally manageable, we chose to use 256 patches. We use the geometry of the best fitting uniform dislocation to obtain, through least squares, an opening distribution that approximates constant pressure. With this prior, we then reoptimize with a constrained least squares algorithm to find the best fitting constant pressure dike. The assumption is that with the prior chosen as described, we are near enough to the global minimum in the new (i.e., constant pressure) misfit space to no longer fear local minimum traps. Hence we abandon the Monte Carlo algorithms in favor of their much more efficient derivative based counterparts.

[17] The primary advantage of using a constant pressure dike is not to lower the misfit, though in fact using these sources does seem to lower the misfit by $\sim 5\%$ over uniform opening dislocations. Rather, the advantage is that a constant pressure dike model is a much more physically realistic representation of the actual intrusive process. Moreover, we have found that placing constraints on the maximum dike pressure, rather than the maximum dike opening,

causes the inversion algorithms to avoid dikes with implausible aspect ratios.

[18] Our preferred model, based on the inversion of the GPS, leveling, and InSAR data, is steeply (80°) dipping to the south, strikes nearly east-west ($N85^\circ W$), is ~ 3 km long and 2 km wide and came to within 500 m of the surface. The driving pressure within the dike was 15 MPa (assuming a shear modulus of 3×10^4 MPa), which corresponds to a maximum opening of 70 cm. The total volume of the dike is 3.3×10^6 m³. The mean square error, which is the weighted residual sum of squares divided by the number of degrees of freedom, was 3.1. Figure 9 depicts the location and geometry of the dike in map view and three-dimensional (3-D) perspective. Note that while the trend of the east rift zone (Figure 1) curves toward the northeast as it approaches the summit caldera, individual dikes in this area have been observed to strike nearly east-west [Klein *et al.*, 1987].

[19] We performed a bootstrap analysis to estimate the uncertainties of and correlations between the model parameters. Following the procedure described by Cervelli *et al.* [2001], we resampled the data vector with replacement and then found the optimal dike source from the resampled data using a constrained least squares algorithm. The results of the bootstrap are depicted in (Figure 10). Figure 10 (bottom) shows the individual confidence intervals for each model parameter; the remainder of the panels show two-dimensional confidence regions for parameter pairs. The orientation of the dike seems very well constrained, as does the driving pressure and horizontal position. Length and width are not uniquely constrained, though the product of the two (dike area) certainly is. These two parameters also seem to trade off with the depth, with deeper dikes seeming to demand longer and narrower dimensions and their shallower counterparts.

4. Discussion

[20] The model dike fits the continuous GPS data, both L1 and dual-frequency, very well (Figure 3). Station NUPM has the most significant misfit, probably because of its proximity to the subsidence from secondary magma chambers in the east rift zone. The campaign data are not so well fit, although at least part of the misfit at stations 69FL and

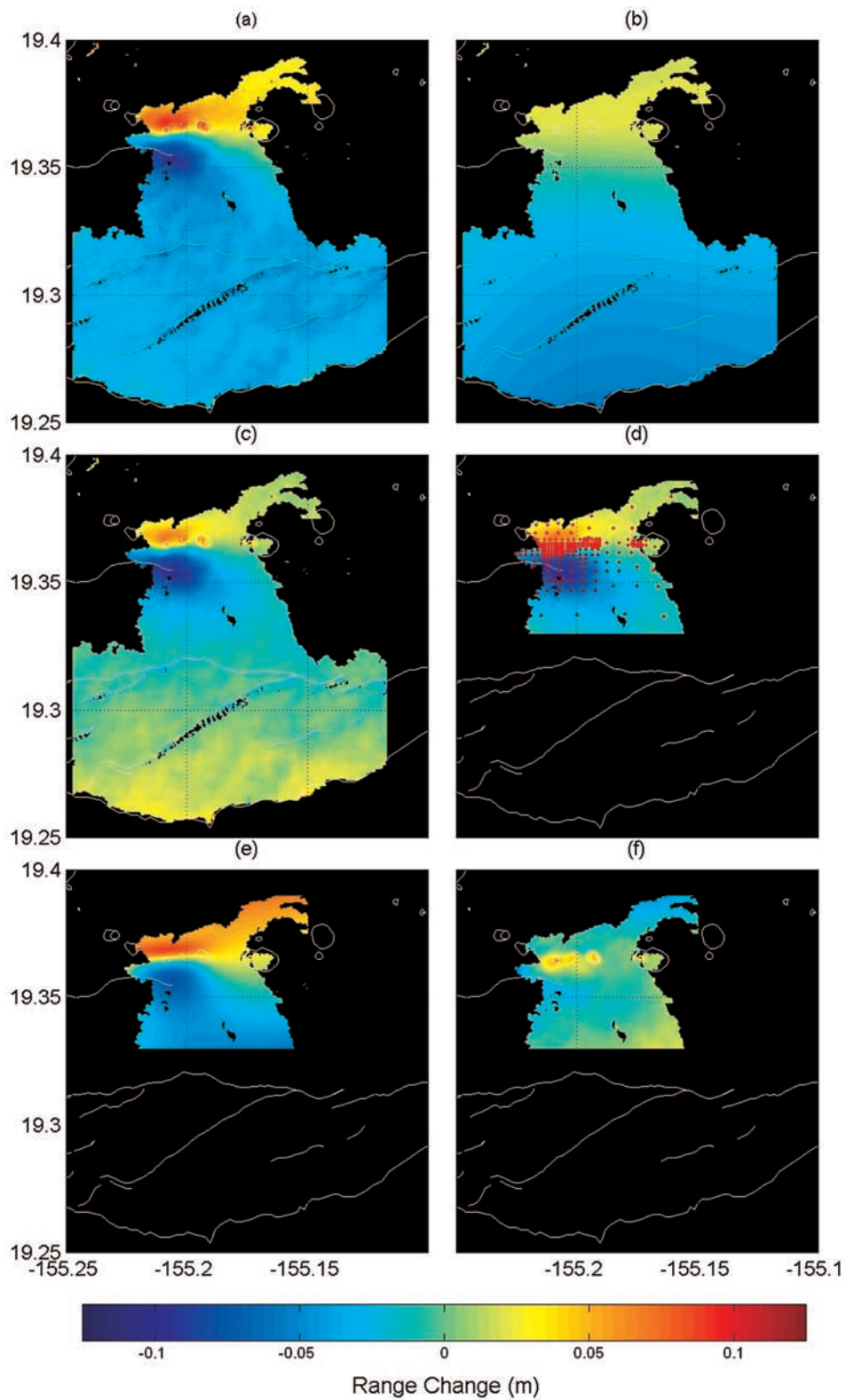


Figure 8. INSAR data. (a) Observed unwrapped range change, (b) trend from *Owen et al.* [2000b], (c) detrended range change, (d) downsized and downsampled data set, (e) model prediction (phase ramp included), and (f) residual.

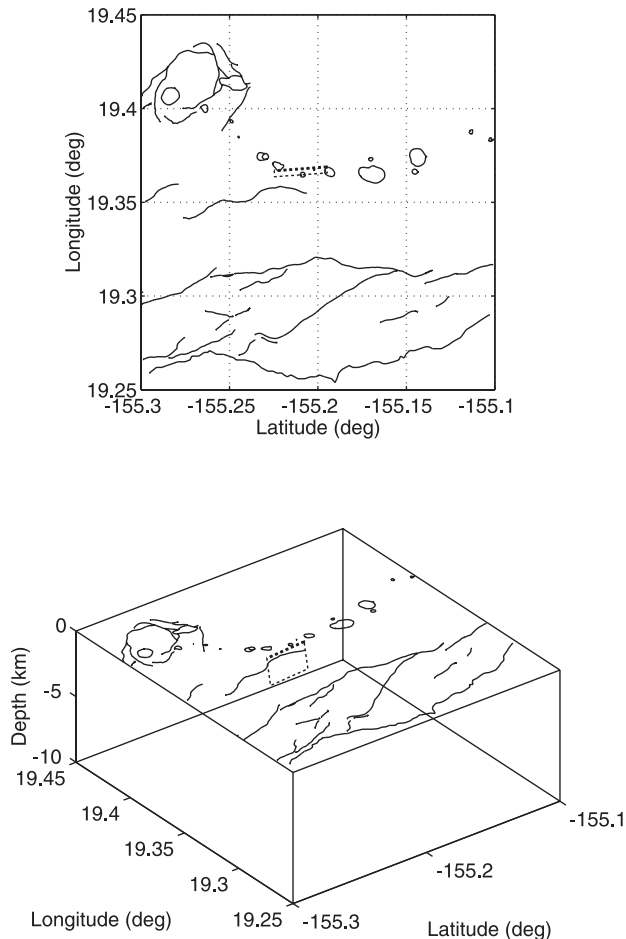


Figure 9. The optimal dike model for the 12 September 1999 intrusion. (top) Map view, (bottom) 3-D perspective.

MULU can be explained by small amounts of slip on the nearby Kalanaokuaiki Pali. Evidence for motion along this fault comes from field observations of ~ 5 mm of surface slip (D. Swanson, personal communication, 2000) and from the appearance of an abrupt discontinuity in the interferogram (Figures 8 and 11).

[21] Figure 7 shows the height changes along the Escape Road leveling line predicted from the model dike. Note that because of the correlations in the leveling data, it is effectively the first spatial derivative of the uplift that is fit, rather than simply the uplift itself. The misfit in the leveling data seems to confirm the observation that the Kalanaokuaiki Pali slipped cointrusively; the major disagreement in slope between observation and prediction occurs precisely where the Kalanaokuaiki Pali crosses the leveling line.

[22] The predicted range changes from the model dike are shown in Figure 8e and the residual in Figure 8f. The residual shows several interesting things. First, there is further evidence of slip on the Kalanaokuaiki Pali since the magnitude of the residual changes abruptly at the trace of the fault (Figure 11 shows this clearly). Second, the craters in this area seem to contain significant areas of misfit within their walls. This could be because the crater floors are moving in response to the intrusion, or it could

be an InSAR processing artifact attributable to the extremely steep crater walls. Finally, the cigar-shaped area of misfit coincident with the surface projection of the model dike probably reveals the shortcomings of our purely elastic model. That is, inelastic deformation is almost certain to have occurred in the region immediately above the dike.

[23] Several authors have noted the interaction between rift zone intrusions and motion of the south flank [Swanson *et al.*, 1976; Delaney *et al.*, 1993]. Indeed, it is widely agreed that Kilauea's rift zones could not exist at all without a mobile south flank to carry away intruded material and keep the stress field in the rift zones conducive to repeated intrusion [Dieterich *et al.*, 1988]. A natural question arises about the relationship between south flank motion and intrusion: Does one of these processes occur as a passive response to the other? Several observations about the deformation associated with September 1999 intrusion may at least partially answer this question: There was no summit inflation prior to the beginning of the earthquake swarm and harmonic tremor that heralded the September 1999 intrusion. This is evident by examining a summit crossing GPS baseline (Figure 12) and the time series of the tiltmeter at Uwekahuna Vault (Figure 2). Nor was there a premonitory increase in the flow rate of magma through the tube system of the active vent (HVO, unpublished data, 1999). These facts suggest that the volume or pressure of the magma in the system did not increase prior to the intrusion. This is consistent with the similar conclusion of Owen *et al.* [2000a] for the January 1997 dike intrusion. It would appear that these dike intrusions into Kilauea's rift zones occurred as a passive response to abrupt failure in the shallow upper crust; that is, the flank motion caused these intrusions.

[24] This lack of premonitory pressurization or inflation is in sharp contrast to some past behavior of Kilauea and Pu'u 'O'o [see, e.g., Wolfe *et al.*, 1987, Figure 17.15], so the description of dike intrusion through passive failure of the rift zones may not typify the long-term history of the volcano. The ongoing eruption at Pu'u 'O'o, fed by an open conduit from the summit magma chamber, appears to limit pressure changes within the magmatic system. This prevents the system from achieving pressures high enough to fracture rock and actively intrude dikes. Whether the conduit remains open and unblocked during periods of sluggish flow may distinguish the past behavior of the system from the current behavior. Early in the Pu'u 'O'o eruption, the walls of the conduit from the summit magma chamber were probably cool relative to the magma flowing past them. This presumably made the system prone to freezing, particularly when the magma (and heat) flux was low. When higher rates of magma flux resumed, the magma could not easily leave the summit area, pressurization ensued and continued until sufficiently high to clear the blocked conduit. The current system is probably much hotter and less prone to freezing, given the nearly 20 years of almost continuous eruption.

[25] The coeval slip on the Kalanaokuaiki Pali may provide tantalizing clues about the mechanics of deformation in this region and perhaps Kilauea's rift zones in general. Did sudden slip on this fault "trigger" the intrusion or was the fault slip a response to the intrusion-induced

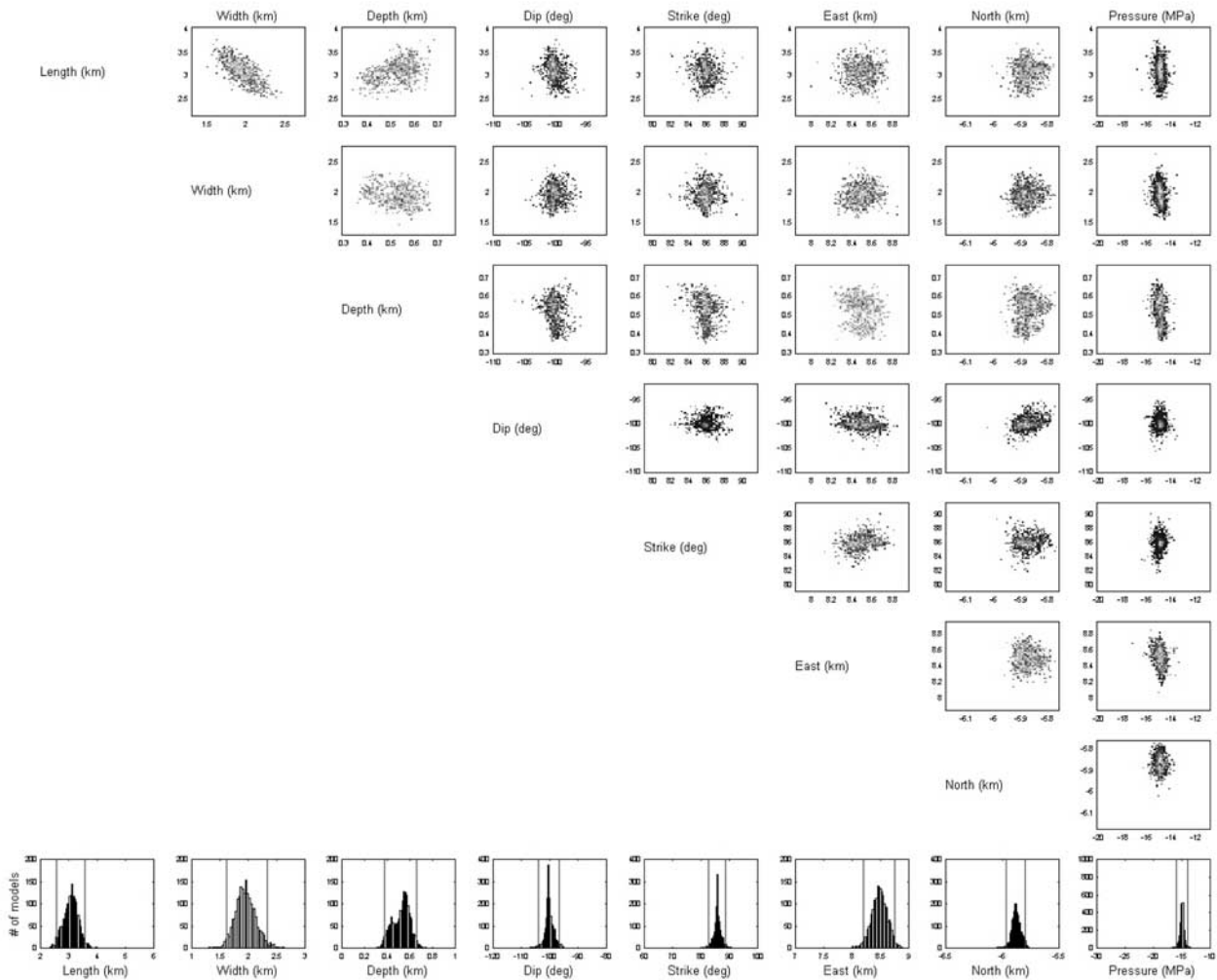


Figure 10. Results of a bootstrap analysis on the 12 September 1999 intrusion. (bottom) Individual confidence intervals for each model parameter; the remainder of the panels show two-dimensional confidence regions for parameter pairs.

stress perturbation? Figure 11 shows the range change measured by InSAR along a north-south transect across the Kalanaokuaiki Pali. The magnitude (~ 1.5 cm) of the sharp jump at the pali is consistent with the observation of slip along this steeply north dipping normal fault. The sense of slip indicated by the range change transect depicted in Figure 11 is normal, with the south side up (i.e., range to satellite decreases). Rubin [1992] discusses graben subsidence and normal fault slip that results from the tensile stress field formed immediately above a propagating dike. While the precise orientation of the fault at depth is not known, a forward calculation based on the final location of the dike shows that the fault likely lies within a zone of increased tension. So, the dike intrusion was probably the proximate cause of the fault slip. The Kalanaokuaiki Pali is a fairly large (~ 5 km), continuous structure, so it is unlikely that it was created by just repeated dike intrusions. Rather, both the existence of the pali and the frequent intrusions are best seen as originating from the long-term effect of deep rifting and seaward sliding along the decollement. Indeed, the dislocation model of Owen *et al.* [2000b] to explain the

long-term GPS velocities predicts a high tensile stress rate in exactly the region of the 1999 intrusion (Figure 13) and the Kalanaokuaiki Pali.

[26] Examination of the tilt time series at the Escape Road station, immediately to the north of the model dike, appears to reveal important information about the direction of dike propagation (Figure 14). In Figures 14b, 14c, and 14d we compare three very simple models of dike propagation: bottom to top, west to east, and east to west, respectively. In each case, we started with the geometry of the best fitting model dike and assumed uniform propagation in each of the three directions. We used unit opening, since we intend to compare these curves qualitatively. However, because the model dike had fairly close to 1 m of opening, it turns out the scales of the forward models are quite close to the observed data. We believe that this analysis strongly favors an interpretation of west to east propagation (Figure 14b). Note that this interpretation captures both the concavity of the north component as well as the sign reversal (presumably as the dike tip propagates by the tiltmeter) of the east component. This

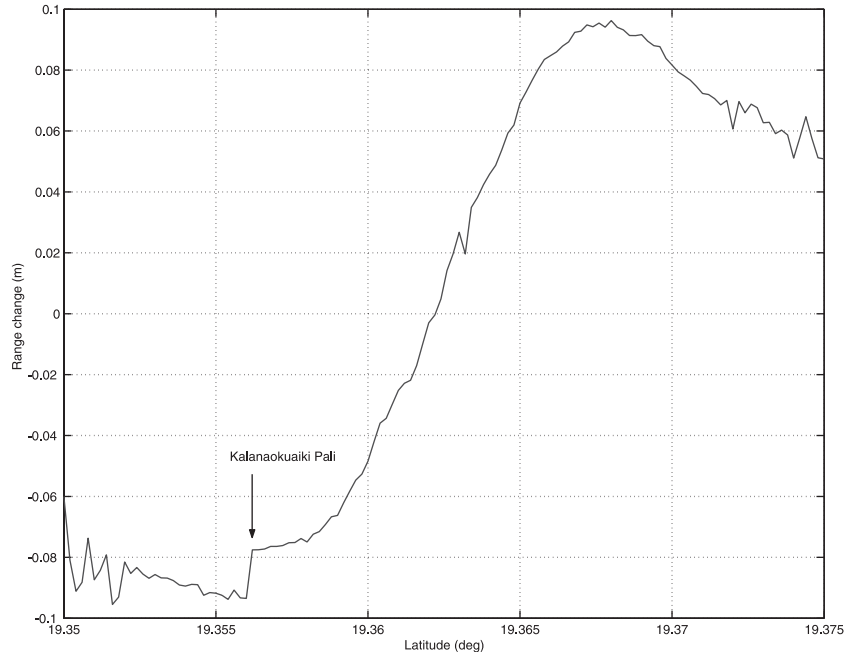


Figure 11. The range changes measured by InSAR along a north-south transect associated with the 12 September 1999 intrusion at Kilauea Volcano. Note the offset at the Kalanaoikuai Pali. The transect runs along the -155.2101 meridian.

interpretation is also consistent with the seismically determined dike propagation directions for dikes in this area. *Klein et al.* [1987] assign a propagation direction for 23 intrusions in the upper east rift zone from 1963 to 1983.

Of these only three show definite uprift (east to west) propagation; seven show propagation in both directions, and the remaining 13 show downrift (west to east) propagation.

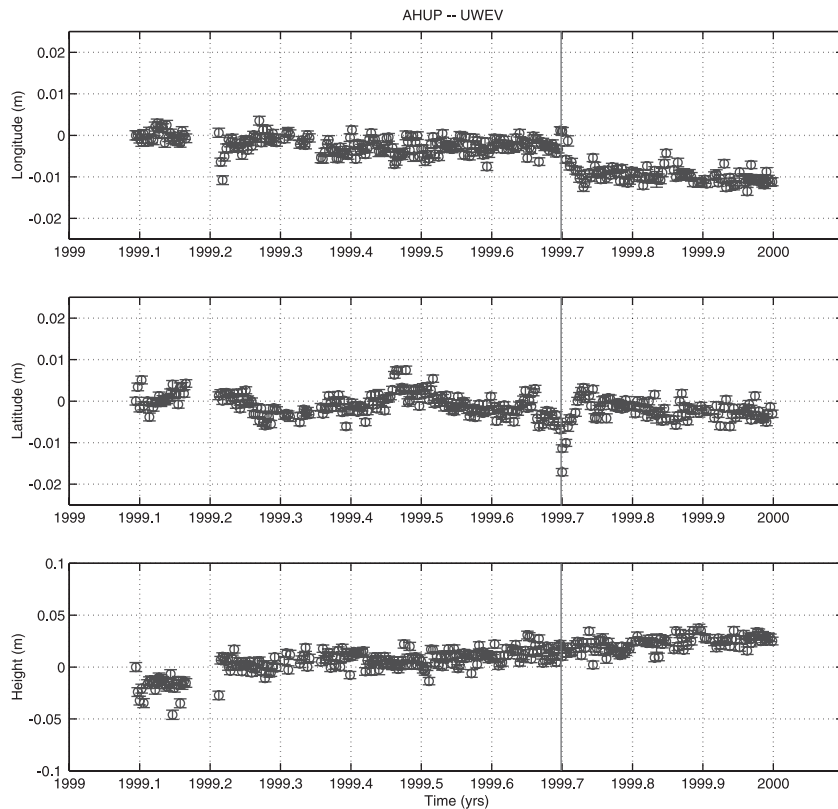


Figure 12. Time series of a summit crossing baseline. There is no evidence of extension across this line that would indicate pressurization of the magma chamber prior to the intrusion (vertical line).

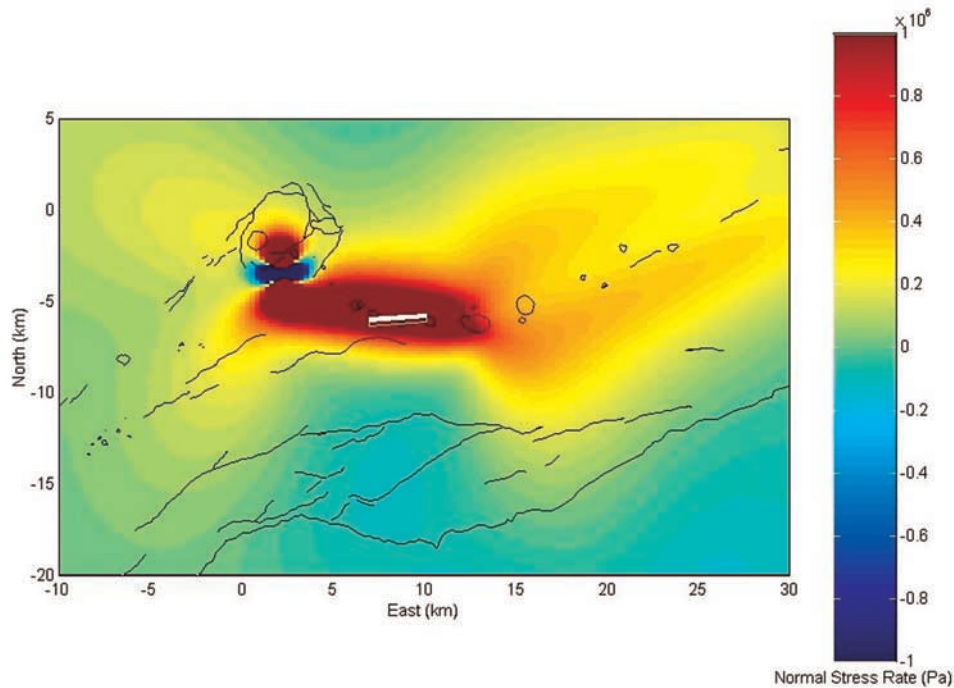


Figure 13. Magnitude of the normal stress rate on dikes in the upper east rift zone at 2 km depth with the same orientation of the 12 September 1999 intrusion. Positive normal stress rates indicate tension; negative rates indicate tension. Stress calculation based on the dislocation model of *Owen et al.* [2000b]. The white box is the surface projection of the 12 September 1999 dike.

[27] The location of the dike and the inferred west to east propagation suggest that the dike's magmatic source probably came from the conduit connecting the summit magma chamber to the Pu'u 'O'o vent. This is consistent

with the widespread draining response seen in the tilt time series (Figure 2) that ranged from the summit all the way to Pu'u 'O'o. However, the magnitude of the tilt signals indicates that these two reservoirs could not possibly have

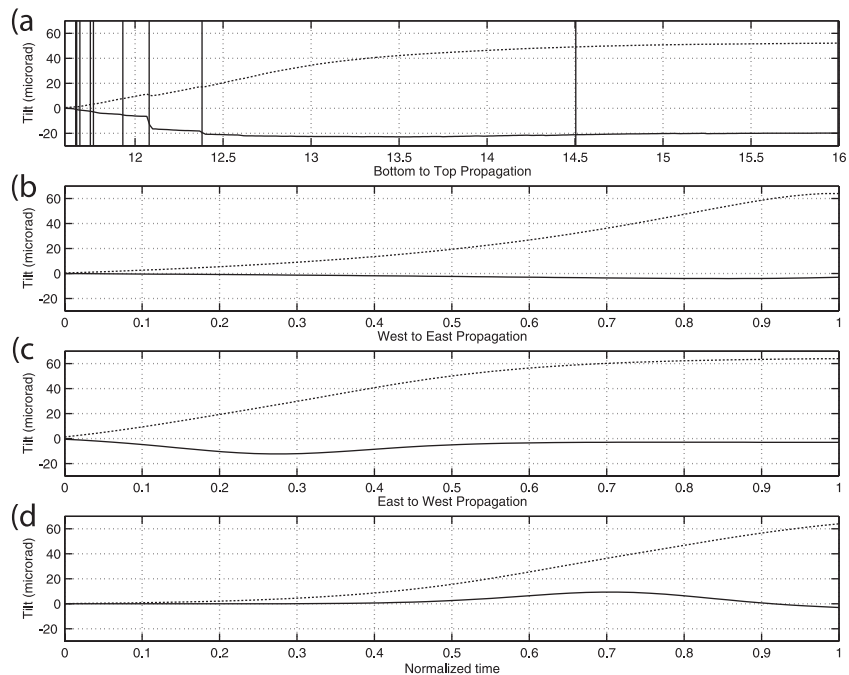


Figure 14. Comparison of various simple models of dike propagation to the tilt time series at Escape Road. (a) Actual data. Dashed line shows the north component of tilt, and solid line shows the east. (b–d) Three models of dike propagation: from bottom to top, from west to east, and from east to west. The west to east propagation model seems to match the actual data best.

supplied the entire volume of magma required to fill the dike intrusion. This strongly suggests the existence of additional shallow magma reservoirs in the upper east rift zone. Reservoirs of this type have been inferred by Owen *et al.* [2000a] to explain the geodetic signal of the January 1997 intrusion and by C. Thornber *et al.* (manuscript in preparation, 2001) based on petrologic data from the erupted lavas of the same event. The magma in the conduit leading from the summit caldera to Pu'u 'O'o probably also contributed to the dike, and if this conduit remained an open cavity after draining, we would expect to see little if any surface deformation. The estimated total volume for the 12 September 1999 dike is $3.3 \times 10^6 \text{ m}^3$. This agrees reasonably well with a nominal magma flux of $4 \times 10^5 \text{ m}^3 \text{ d}^{-1}$ [Thornber *et al.*, 1997] times the pause length of 11 days, suggesting that only once the magmatic system returned to its preintrusive state could the eruption at Pu'u 'O'o resume.

5. Conclusions

[28] The 12 September 1999 earthquake swarm in the upper east rift zone of Kilauea Volcano was caused by an east-west striking dike that dips steeply to the south and intruded just to the east of Mauna Ulu. The region of the intrusion is characterized by high tensile stress caused by the persistent deep rifting in the east rift zone and by continued seaward sliding of the south flank along a basal decollement. The high stresses eventually lead to failure in the shallow crust above the deep rift zones, which permits opportunistic emplacement of dikes into the failure area. The source of magma for these opportunistic intrusions comes from the summit magma chamber, a smaller chamber beneath Pu'u 'O'o, and from the conduit that connects the two. Smaller pockets of old magma residing in the upper east rift zone may also contribute to the dike volume. These passive intrusions probably represent the only means by which dikes can form in the current state of the volcanic system at Kilauea; the stable, open conduit to Pu'u 'O'o limits the amount of magma pressure that can accumulate, effectively ruling out forcible active intrusions. However, a suddenly increased flux of magma into the summit magma chamber could overwhelm the capacity of the current conduit system causing not only vigorous eruption at Pu'u 'O'o but also perhaps eruption or intrusion at the summit itself or within the Southwest Rift Zone.

[29] **Acknowledgments.** We would like to thank Michael Bevis and his research group at the University of Hawaii for access to the data from UH Continuous GPS network on Kilauea Volcano. Funding for this research was provided by the National Science Foundation and the National Aeronautics and Space Administration.

References

- Árnadóttir, T., P. Segall, and M. Matthews, Resolving the discrepancy between geodetic and seismic fault models for the 1989 Loma Prieta, California, earthquake, *Bull. Seismol. Soc. Am.*, **82**, 2248–2255, 1992.
- Cervelli, P., M. Murray, P. Segall, Y. Aoki, and T. Kato, Estimating source parameters from deformation data, with an application to the March 1997 earthquake swarm off the Izu Peninsula, Japan, *J. Geophys. Res.*, **106**, 11,217–11,238, 2001.
- Delaney, P. T., A. Miklius, T. Arnadóttir, A. T. Okamura, and M. K. Sako, Motion of Kilauea Volcano during sustained eruption from the Pu'u 'O'o and Kupaianaha vents, 1983–1991, *J. Geophys. Res.*, **98**, 17,801–17,820, 1993.
- Dieterich, J. H., Growth and persistence of Hawaiian rift zones, *J. Geophys. Res.*, **93**, 4258–4270, 1988.
- Klein, F. W., R. Y. Koyanagi, J. S. Nakata, and W. R. Tanigawa, The seismicity of Kilauea's magma system, in *Volcanism in Hawaii*, edited by R. W. Decker, T. L. Wright, and P. H. Stauffer, *U.S. Geol. Surv. Prof. Pap.*, **1350**, 961–996, 1987.
- Okada, Y., Surface deformation due to shear and tensile faults in a half-space, *Bull. Seismol. Soc. Am.*, **75**, 1135–1154, 1985.
- Okada, Y., Internal deformation due to shear and tensile faults in a half-space, *Bull. Seismol. Soc. Am.*, **82**, 1018–1040, 1992.
- Owen, S., P. Segall, M. Lisowski, A. Miklius, M. Murray, M. Bevis, and J. Foster, The January 30, 1997 eruptive event on Kilauea Volcano, Hawaii, as monitored by continuous GPS, *Geophys. Res. Lett.*, **27**, 2757–2760, 2000a.
- Owen, S., P. Segall, M. Lisowski, A. Miklius, R. Denlinger, and M. Sako, Rapid deformation of Kilauea Volcano: GPS measurements between 1990 and 1996, *J. Geophys. Res.*, **105**, 18,983–18,998, 2000b.
- Rubin, A. M., Dike-induced faulting and graben subsidence in volcanic rift zones, *J. Geophys. Res.*, **97**, 1839–1858, 1992.
- Swanson, D. A., W. A. Duffield, and R. S. Fiske, Displacement of the south flank of Kilauea Volcano: The result of forceful intrusion of magma into the rift zones, *U.S. Geol. Surv. Prof. Pap.*, **963**, 39 pp., 1976.
- Thornber, C., D. Sherrod, C. Heliker, J. Kauahikaua, F. Trusdell, M. Lisowski, and P. Okubo, Kilauea's ongoing eruption: Napau Crater revisited after 14 years (abstract), *Eos Trans. AGU*, **78**(17), Spring Meet. Suppl., S329, 1997.
- Welstead, S. T., *Fractal and Wavelet Image Compression Techniques*, 232 pp., SPIE Opt. Eng. Press, Bellingham, Wash., 1999.
- Wolfe, E. W., M. O. Garcia, D. B. Jackson, R. Y. Koyanagi, C. A. Neal, and A. T. Okamura, The Pu'u 'O'o eruption of Kilauea Volcano, episodes 1–20, January 3, 1983 to June 8, 1984, in *Volcanism in Hawaii*, edited by R. W. Decker, T. L. Wright, and P. H. Stauffer, *U.S. Geol. Surv. Prof. Pap.*, **1350**, 961–996, 1987.
- Zumberge, J. F., M. B. Heffline, D. C. Jefferson, M. M. Watkins, and F. H. Webb, Precise point positioning for the efficient and robust analysis of GPS data from large networks, *J. Geophys. Res.*, **102**, 5005–5017, 1997.
- F. Amelung and H. Garbeil, Department of Geology and Geophysics, University of Hawaii at Manoa, Honolulu, HI 96822, USA. (amelung@hawaii.edu)
- P. Cervelli and A. Miklius, U.S. Geological Survey, Hawaiian Volcano Observatory, P.O. Box 51, Hawaii National Park, HI 96718, USA. (pcervelli@usgs.gov; asta@usgs.gov)
- P. Segall, Department of Geophysics, Stanford University, Mitchell Bldg. B17, Stanford, CA 94305-2215, USA. (cervelli@stanford.edu; segall@stanford.edu)
- M. Lisowski, U.S. Geological Survey, Cascades Volcano Observatory, 1300 SE Cardinal Court 100, Vancouver, WA 98683-9589, USA. (mlisowski@usgs.gov)
- C. Meertens, University NAVSTAR Consortium, 3340 Mitchell Lane, Boulder, CO 80301, USA. (chuckm@unavco.ucar.edu)
- S. Owen, Department of Earth Sciences, University of Southern California, Los Angeles, CA 90089-0740, USA. (owen@earth.usc.edu)